Journal of Nuclear Materials 447 (2014) 225–232

Contents lists available at ScienceDirect

Journal of Nuclear Materials

journal homepage: www.elsevier.com/locate/jnucmat

In situ resistivity measurements of RAFM base alloys at cryogenic temperatures: The effect of proton irradiation

B. Gómez-Ferrer [a,b,*], R. Vila [a], D. Jiménez-Rey [b], C.J. Ortiz [a], F. Mota [a], J.M. García [a], A. Rodríguez [b]

[a] Euratom/CIEMAT Association, Avenida Complutense 22, 28040 Madrid, Spain
[b] Centro de Micro-Análisis de Materiales (CMAM), Universidad Autónoma Madrid, 28049 Madrid, Spain

ARTICLE INFO

Article history:
Received 29 July 2013
Accepted 13 January 2014
Available online 22 January 2014

ABSTRACT

A four-probe technique for measurement of electrical resistance on low-temperature ion-irradiated metallic sheets is described. The design, temperature control system, preparation method of samples and the resistivity measurements are described in detail. The resistivity recovery (RR) curve has been measured on a Fe–5%Cr model alloy irradiated with 5 MeV protons. The procedure to obtain the RR derivative curve is outlined and experimental errors are identified and quantified. Special care has been taken to use a sample with very low impurity content and low dislocation density (1.2×10^8 cm^{-2}). Thus, effects in recovery spectrum of the Fe–5%Cr alloy are only due to the presence of Cr and irradiation defects, which will be mainly Frenkel Pairs (FPs) given that the mean energy of the Primary Knock-on Atoms (PKA) is close to 0.35 keV. The results obtained for the Fe–5%Cr under 5 MeV proton irradiation are found to be in overall agreement with previous experimental measurements performed under electron irradiation although some differences appear probably due to the different spatial distribution of the created defects and the higher temperature resolution of annealing steps. The RR spectrum obtained reveals the appearance of the structure of stages I and II and also a partial suppression of the stage III peak with respect to previous results obtained after electron irradiation. The stage III suppression is explained as a superposition of vacancy recombination effects and short-range ordering (SRO) effects which are apparently dependent on the spatial distribution of defects created during irradiation. Moreover, recombination phenomena are observed beyond stage III up to 500 K.

1. Introduction

Development of nuclear materials capable to withstand hostile environments is one of the principal challenges facing the development of future nuclear reactors. In particular, structural materials of future fusion reactors will be exposed to intense high-energy neutrons, electrons, ions and electromagnetic irradiation as a consequence of fusion reactions in the hot plasma. This radiation will produce a significant amount of defects in the structure of the materials, affecting their physical properties at different scales, and hence, their reliability as structural materials.

In order to identify suitable structural materials for fusion reactors and establish boundary conditions for such materials in operation, it is crucial to fully understand the radiation effects, which can be done using a physically-based modelling approach. This can be achieved undertaking computational simulations to reproduce well-designed experiments carried out under well controlled irradiation conditions and on model alloys. This method allows validating parts of our models and can provide additional information on the atomistic mechanisms responsible for defect evolution. This approach is non-straightforward and strong efforts are still needed to develop the models and to obtain new experimental data.

When it comes to structural materials, it is well known that reduced activation ferritic/martensitic steels (RAFM) are the most promising candidates for fusion and fission applications. Its optimized Cr concentration (typically ~9%) reduces swelling, radiation-induced ductile–brittle transition temperature (DBTT) [1,2] and increases protection against corrosion [3]. It is postulated that trapping of interstitials and interstitial clusters due to Cr atoms in Fe alloys might explain the reduced swelling and enhanced nucleation of interstitial loops compared to pure Fe [4]. Nevertheless micro-structural mechanisms responsible for such behaviour and its evolution under irradiation are still not well understood and detailed study of $FeCr_x$ based alloys is still required. The resistivity recovery (RR) measurements can be used as a validation tool to study basic physics of point defects in $FeCr_x$ systems and this has been the case, as this method has been widely used [5–8] because

* Corresponding author. Address: Avda. Complutense 40, Ed.2 – P0 – 28L, 28040 Madrid, Spain. Tel.: +34 914962574; fax: +34 913466068.
E-mail address: begona.gomez-ferrer@externos.ciemat.es (B. Gómez-Ferrer).

http://dx.doi.org/10.1016/j.jnucmat.2014.01.016
0022-3115/

of its high sensitivity to the presence of defects in metals. RR measurements can isolate the effects of irradiation defects as they are usually performed at cryogenic temperatures. Thus the electron–phonon interaction is suppressed and the measured resistivity values only depend on the ordering of the material microstructure, i.e., the residual resistivity. The cryogenics condition requires performing *in situ* measurements where residual resistivity values can be obtained before, during and after irradiation and also after temperature cycles. Measuring the radiation-induced resistivity of the microstructure of irradiated Fe and $FeCr_x$ alloys allows correlating defect production with irradiation parameters, in particular dose and energy. In addition, the follow-up of damage during post-irradiation annealing provides valuable information on defect kinetics, their diffusion, recombination and clustering.

As suitable 14 MeV neutron sources are not yet available for material studies, research has been mainly centred on the use of electron irradiations which produce mainly spatially separated FPs. One of the advantages of this type of irradiation is that initial conditions are relatively easy to define in simulation set-up. Thus, using electron irradiation and combining RR experiments [5], positron annihilation (PA) experiments [9] and simulations, which combine Molecular Dynamics (MD), kinetic Monte-Carlo (kMC) and Rate Theory [10], it was possible to shed light on fundamental aspects of defect kinetics in pure Fe. Concerning Fe alloys, it has been shown that the presence of solutes exhibits strong interaction with point defects, which complicates the interpretation of RR stages in terms of defect kinetics. Particularly in bcc Fe–Cr alloys it has been determined that Cr solutes tend to trap self-interstitial atoms (SIA), but, do not interact with vacancies (V) [11]. Thus, the migration mechanisms of very simple defects, such as interstitials, vacancies and their small clusters change with respect to pure Fe. Also, in binary alloys the long range migration of simple defects enhances the rearrangement of solutes, leading to changes in the residual resistivity. Such re-ordering is the so-called short-range ordering (SRO) and can lead to increase or decrease of residual resistivity values as a function of the sign of the Cowley–Warren SRO parameters [12,13]. All these questions, the limited experimental data available [11,14–18] and the current limitations of computing models and codes stresses the need to continue to perform new well controlled experiments to understand the physics of $FeCr_x$ RR spectra.

Up to date most resistivity and positron annihilation experiments for understanding the behaviour of RAFM based alloys have been carried out under electron irradiation [5,8,11,14–17,19–21]. It is worth noting that in this work the irradiation of samples was carried out with 5 MeV protons, which allows to study the behaviour of steel microstructure under a type of irradiation damage different from the one generated by electrons but closer to what neutrons would create. As it is shown in the discussion, this is going to reveal new processes on the RR results.In this work, a pure Fe–5%Cr specimen was irradiated by 5 MeV protons at 50 K. The defects created during irradiation contribute to the so-called radiation induced resistivity (RIR) which is measured at a temperature of 20 K. After irradiation, the sample temperature was raised up by successive temperature steps and then cooled down again to base temperature (T_{base} = 30 K) in order to perform all the residual resistivity measurements after annealing up to 500 K. The RR curve was obtained with this procedure and its derivative provides the RR spectrum where the stages I, II and III can be identified.

In Section 2 we first describe the studied material and its preparation, the experimental set-up, the irradiation and finally the measurement proceeding. Section 3 is dedicated to the theoretical calculation of the damage produced by proton irradiation, which will set the basis for the discussion of the experimental results. We then present the results obtained and the analysis method in Section 4. Finally, a comparison with previous measurements performed with electron irradiation is presented and discussed.

2. Experimental

In this section the requirements and difficulties for undertaking RR measurements on samples irradiated at cryogenic temperatures are outlined. An explanation of experimental details highlighting the technological difficulties needed to be overcome in such experiments is interesting in order to understand the reliability and comparability among results from different authors. In particular, the design of the sample holder which assembles all the systems for resistivity measurements, heating and temperature monitoring is carefully described as it is a fundamental piece to guarantee the success of the RR measurements. The system described here was developed in order to irradiate thin metal alloy foils using protons of some MeV's at cryogenic temperatures in order to achieve an almost homogeneous damage in the bulk of the order of 10^{-4} displacement per atom (dpa). Then, once irradiated, the residual resistivity of the sample is monitored near liquid He (LHe) temperatures along a step-like annealing process. The measurements were undertaken at the 5 MV Tandetron accelerator of CMAM (Centro de Micro-Análisis de Materiales) [22]. A 5 MeV proton beam with a current of 30 nA was used to assure a negligible sample heating, so a total sample irradiation time of 2.5 h was needed to achieve the desired dose.

The basic requirements for achieving reliable RR measurements are the following:

- A thin sample with well controlled microstructure and impurity content.
- An experimental chamber for irradiation at cryogenic temperatures with an *ad hoc* sample holder.
- A reliable system for monitoring and control the sample temperature (crucial issue).
- An *in situ* analysis technique for the resistivity measurements and the temperature cycles.
- A suitable proton beam and its associated beam control systems.

2.1. Material and sample preparation

Fulfilment of required experimental conditions (bulk uniform irradiation, high temperature range from cryogenics to 500 K, low-voltage measurements and temperature cycling) together with sensitive subsequent treatment of the experimental data (derivative of the experimental curve) makes RR experiments difficult to perform. Several authors have developed experimental RR systems for wire-like and bridge-type [23] samples of tens to hundreds of μm thickness [5,8,11,15,20,24,25]. In such cases, the sample preparation methods used involved mechanising processes that may alter the microstructure and composition of the departing material and thus give rise to unclear results. In the present work we wanted to avoid cold-rolling to prepare the specimens in order to guarantee that the purity, grain size, Cr distribution and low dislocation density of the departing material is maintained. The chromium ferritic/martensitic base alloy used was designed in the framework of EFDA contract [26,27] and provided by "ÍEcole Nationale Supérieure des Mines" (CNRS) in the form of small bars of 10.9 mm of diameter. The Fe–5%Cr was recrystallized after cold reduction of 70% and then heat treated for 1 h under pure Ar flow at 1023 K. Table 1 lists the composition, the annealing temperature, the mean grain size and the dislocation density of the irradiated alloy. The four-lead van der Pauw (VdP) technique [28] was thus chosen for measuring the resistivity. The method assumes that samples are homogeneous, isotropic, and two-dimensional (thickness small compared to breadth and width) and that the sample boundaries are sharply defined. The "clover-leaf" geometry

Table 1
Detailed microstructure of studied material: impurity content (ppm), grain size and dislocation density.

Composition and microstructure	Fe–5%Cr
C	3
O	6
S	3
N	3
P	<5
Cr	5.40 wt%
Annealing temperature	750 °C
Mean grain size	68 μm
Dislocation density	1.2×10^8 cm^{-2}

of the sample allows maximum profit of the slices cut from the departing bars, avoiding highly damaging mechanising processes. In the ASTM standards it is recommended for samples of arbitrary shape [23], resulting in a less strict configuration concerning the sample dimensions and probe position (as it is in the bridge configuration). It is also recommended in order to reduce any errors due to non-ideal contacts [28–30] and to improve the geometric factor (this is the factor which relates the electrical resistance with the resistivity and usually depends on the shape of the sample and the position of the electrodes). The measurement results are then independent of the wanderings of probes in a region near the border and therefore it is unnecessary to determine the precise positions of probes in order to make corrections for the boundary effect [31].

In addition, the samples need to be sufficiently thin in order to ensure quite uniform bulk irradiation while simultaneously allowing bulk resistivity measurements to be made (minimizing surface effects). In order to obtain a homogeneous distribution of damage throughout the bulk with energetic protons, samples have to be thin enough so that the Bragg's peak is well beyond the thickness of the sample. For 5 MeV protons this condition determines a maximum thickness of 70 μm according to SRIM simulations [32]. Thus, a ~50 μm plane-parallel foil was obtained from the delivered bars while minimizing alterations to the microstructure.

The sample preparation process to obtain "clover-leaf" 50 μm samples was designed to minimize any modifications to the microstructure of the departing material. Firstly, 0.5–1 mm thick slices were cut by spark erosion from the original bars and then 4 clefts where performed using the same technique to obtain the "clover leaf" shape. Next, the thin overlying oxide layer was removed using a low temperature (−20 °C) electrochemical process with ethanol and perchloric acid. Then, the samples were grinded using 320, 600, 1200 and 2500 paper-grit. Finally, they were polished on a plane-parallel automatic polishing machine, employing diamond suspensions from 3 to 0.25 μm. Eventually, the size of the specimens was ~50 μm thick with a mirror-like surface finish. Although mechanical polishing can induce a damage deformation surface in some cases, deformation-free surfaces can be obtained by correct choice of the cutting device (manual or automatic), polishing methods (purely mechanical or chemical–mechanical process) and abrasives used [33,34]. Indeed the ⩽3 μm grade of polycrystalline diamond used here as the carrier paste added to a short-nap cloth produced a surface with a shallow low-strain-damaged layer which eventually should be neglected with respect to the bulk of the sample. Electrochemical polishing was also considered as the final treatment to remove possible surface mechanical stresses but after several tests it was rejected given that control over the geometry of the sample was not accurate and plane-parallelism and shape where degraded. Concerning thermal treatments, some tests were done in vacuum conditions, but the appearance of a thin oxidation layer on the surfaces was considered to be much worse than the few nanometer damage produced by the mechanical polishing. From these considerations we ruled out the use of cold-rolling techniques to produce a long rectangular sample, as this method needs a high temperature thermal treatment to remove the huge damage produced. Considering the 50 μm thickness, this treatment could alter the original microstructure, the SRO parameter and can segregate Cr ions to the surface.

2.2. Experimental set-up

In order to perform the experiments proposed, a dedicated test chamber was designed, built and installed in a line of the ion accelerator of CMAM. The test chamber was designed in such a way that sample can be irradiated while performing resistivity measurements, monitoring and controlling the temperature of the sample simultaneously. The set-up for the experiment undertaken here consisted in placing the sample at the end of the cold finger of a continuum flow cryostat; model ST-400by Janis Research Co. (Wilmington, MA), together with an oven, a temperature control system and corresponding electrical connections for the resistivity measurements. The cryostat is attached to the top of the experimental chamber. In addition, there is a rotary feedthrough on this top which holds ionoluminescent quartz in front of the sample before starting the irradiation in order to determine the position, size and homogeneity of the proton beam. With this system, '*in situ*' cooling down, irradiation, isochronal annealing and resistivity measurements can be done, avoiding post-irradiated manipulation of the sample.

The cryostat was accommodated to a vacuum chamber. Feedthroughs provide connections for electrical and temperature measurements. As standard inner temperature controls, the cryostat includes one high temperature (500 K) standard curve silicon diode and a 50 Ω cartridge heater. The cold finger is protected with an adjustable height gold plated OFHC Copper radiation shield 3.3 cm O.D. The specimen holder (see Fig. 1) assembles all the systems for

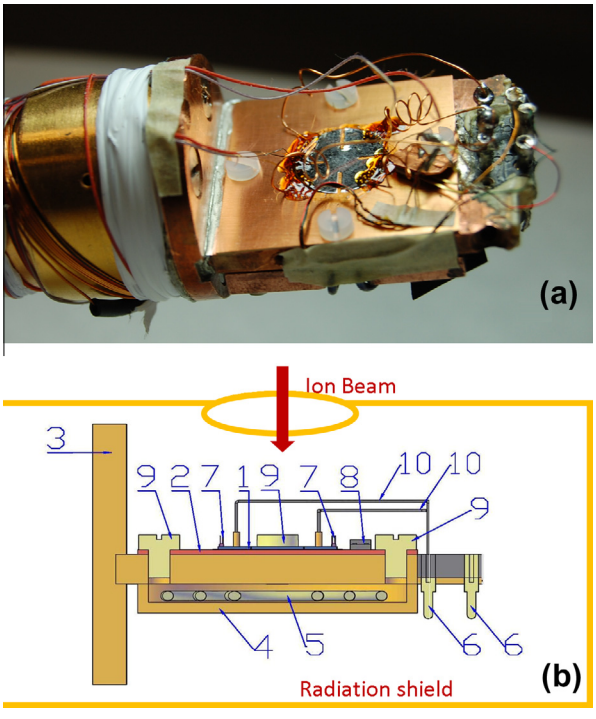

Fig. 1. (a) The sample holder, without the radiation shield, as mounted on the cold finger. (b) A cross-sectional profile of the sample holder: 1. Sample – 2. Cu plate with a deposited layer of SiO_2 – 3. OFHC Cu sample holder which adapts to the cryostat cold finger – 4. Copper holder which contains the heater – 5. Thermocoax® heater – 6. Pin-like intermediate connectors – 7. Type *E* thermocouples – 8. Silicon diode – 9. Nylon screws – 10. Electrical connections for resistivity.

measurement, heating and control. The sample holder system had to handle a wide range of temperatures, i.e. from liquid helium up to 500 K. This implied that good contact at the thermal boundaries (between the heat sink and the sample) had to be maintained over a range of ~500 K. Also the metallic sample had to be electrically isolated from the rest of the system but at the same time a good thermal conductivity between sample and warm and cool sources was required in order to get an accurate and robust temperature control. Variations of resistivity due to irradiation are in the order of hundreds of $n\Omega$ cm and variations of resistivity due to temperature changes (near LHe) are two orders of magnitude smaller ($\Delta\rho$ ~8 $n\Omega$ cm, per degree at 30 K), thus the control of temperature at the sample has to be very sensitive and stable, otherwise large experimental error could be amplified during the calculation of the derivative of the RR curve. The sample holder is made of OFHC cooper and fixed to the end of the cold finger with screws and indium foil. For easy and non-damaging handling, the sample is stuck with varnish GE-7031 to a thin (0.3 mm) cooper plate. This varnish was tested under ion-irradiation and was able to withstand high ion fluxes before being denatured. The plate is covered by a sputtered thin film of SiO_2 which makes the surface electrically isolating but keeps good thermal conducting at low temperatures. The four-probe electrical connections were made by spot welding on the edges of the sample. Four cooper AWG32 wires link the sample with an intermediate pin-like connector on the sample holder. Two type E thermocouples are spot welded at the upper and lower edges of the sample respectively in order to determine the sample temperature and any possible temperature gradient along it. Also, since thermocouples may not be totally reliable at the very low temperatures employed, a silicon diode is attached to the plate close to the sample. It should also be noted that, as described before, an additional silicon diode is placed inside the cold finger of the cryostat in order to achieve good temperature control of the heat sink. Finally, the heat source for raising the sample temperature is a coaxial cable electrical heater (11 Ω) which is placed at the rear part of the sample holder. All the temperature probes, the four-probe sample connections and the heater are connected to their respective UHV feedthroughs by thermally anchored suitable extension cables.

Once the sample is placed on the cold-finger, the whole system is placed in a vacuum chamber at the end of one of the beam line of the ion accelerator. During irradiation the collimated ion beam passes through a 15 mm diameter hole in the radiation shield and impacts the sample. The beam current of 30 nA (for samples of 50 μm) was used in order to minimize the increase in sample temperature during irradiation (T_{irr}, ~50 K). In order to measure the beam current with accuracy, two independent devices where used: a Faraday cup and a transmission Faraday cup. They were placed in the irradiation line before the vacuum chamber, as it can be seen in Fig. 2, which pictures schematically the whole assembly in the beam line. Concerning the beam shape, an over focused homogenous irradiation area (around 6.5 × 6.5 mm^2) into the sample was carried out. The beam positioning, and its homogeneity, was set using the ionoluminescence from a fused silica plate that was placed temporarily in front of the sample on a rotary feedthrough.

2.3. Resistivity and temperature measurements

Electrical measurements were made in DC mode with the 4-point-probe method in the VdP configuration [28]. The resistivity of the sample has to be measured in configurations R_{12} and R_{23} as shown in Fig. 3. Current and voltage leads where connected to a high precision current source (model 6221 by Keithley Instruments Inc., Cleveland, OH) and to a nano-voltmeter (model 2182A by Keithley Instruments Inc., Cleveland, OH) which were connected to each other with an RS-232 bus and a trigger link.

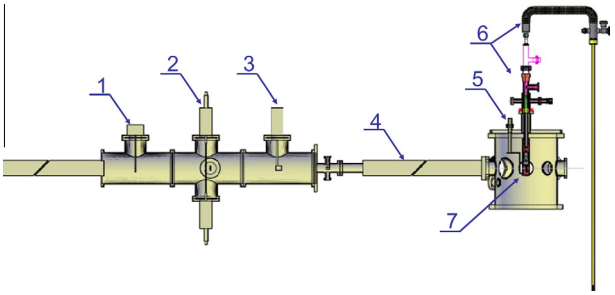

Fig. 2. Beam alignment and irradiation set-up: 1. Transmission Faraday cup – 2. Collimation slits – 3. Faraday cup – 4. Beam line – 5. Rotary feedthrough with ionoluminescent quartz – 6. Cryostat and LHe transfer line – 7. Sample holder.

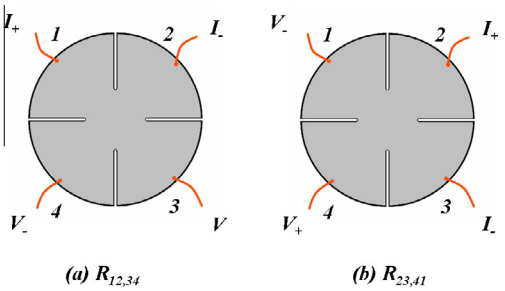

Fig. 3. (a) R_{12} probe configuration for VdP: current passes through probes 1 and 2 and voltage drop is measured between 3 and 4. (b) R_{23} configuration: current is applied to probes 2 and 3, and voltage is measured between 4 and 1.

Combination of such current source and nano-voltmeter was used to perform delta mode, that is, a delta current-reversal technique that is used to cancel the effects of thermal EMFs [35]. The sample voltage is measured with an accuracy of 10^{-8} V while applying 100 mA (±0.1%). When considering the standard deviation of the experimental value (at a given temperature) it is in the order of 1–0.1 $n\Omega$ cm, thus for measuring resistivity differences, the standard deviation is the error considered. Reproducibility of the resistivity values strongly depends on the stability of the sample temperature, so 1 $n\Omega$ cm accuracy corresponds to a 0.1 K of uncertainty (at 30 K). It must be noted that measurement of the true sample temperature while resistivity is being measured is always a challenge at these low temperatures. In the current set-up, the only sensors that maintain contact with the sample are the spot-welded thermocouples. However, as thermocouples are not very reliable at temperatures below 77 K, an alternative silicon diode was placed over the Cu plate and separated from the sample by only 1 mm (see Fig. 1). This sensor is used to control the base temperature for the measurements with the proportional-integral derivative (PID) controller. In order to make clear the orders of magnitude, Table 2 summarizes values and errors of resistivity and temperatures measured with each sensor in the set-up. It also must be noted that the temperature sensors were tested in a LN bath in order to check its good performance under isothermal conditions at low temperature.

RIR measurements where performed at minimum temperature in the cryostat and RR measurements at a base temperature (T_{base}) of ~30 K. The RR curves where obtained along step-like annealing procedure: the temperature was raised in steps of 2.5 K between 50 and 90 K, $\Delta T/T = 0.03$ from 90 to 400 K and 20 K steps above 400 K. The temperature ramps had a rising velocity of 10 K/min and annealing time is $\Delta t = 120$ s. The ultimate annealing temperature reached was close to 500 K and the complete annealing and measurement process took over 60 h after irradiation. It is worth noting that the key point for measuring RR curves is to understand

Table 2
Values for a sample of Fe–5%Cr: ρ is the resistivity of the sample, T_{SD670} is the temperature of the silicon diode placed on the sample holder, T_{TC} is the temperature read by the thermocouples and $T_{ID\ ST\text{-}400}$ is the temperature of the inner diode of the cryostat ST-400.

	ρ ($n\Omega$ cm)	T_{SD670} (K)	T_{TC} (K)	$T_{ID\ ST\text{-}400}$ (K)
RT	33033.1 ± 0.9	300.0706 ± 0.0002	299.47 ± 0.07	300.234 ± 0.008
Base T	10367.5 ± 1.2	11.331 ± 0.012	29.78 ± 0.18	4.53 ± 0.09
Min. T in cryostat	9893.0 ± 0.6	7.676 ± 0.002	23.27 ± 0.11	4.0235 ± 0.0014
HeL immersion	9864.5 ± 1.1[a]	4.23903 ± 0.00005	–	–

[a] Minimum error in resistivity should be found during the HeL immersion test because of the strong stability of the temperature, nevertheless as the sample was directly in the HeL device without correct shielding of the electric cables, the error is higher than expected.

how well the system is capable of returning to the base T_{base} after cycling, bearing in mind that as the annealing proceeds, the LHe flow can vary and also the spot-welded electrical connections and thermal boundaries could be slightly modified due to the temperature cycles. In order to estimate a more representative value of the resistivity error, a value of twice the standard deviation of the first points of the annealing process (30–55 K) where recovery can be barely appreciated has been taken; giving a value of 3 $n\Omega$ cm. This provides an upper limit value for error but it is considered a better estimate of the whole experimental errors commented above.

The reproducibility of the RR data has been checked and an example of stage I is shown in the insert of Fig. 6. This first stage of the RR spectrum where more errors normally appear is well reproduced and also small sub-stages before main stage I_D are revealed (see Section 5 and Figs. 6 and 8). Such sub-stages have not been shown in other experiments due to the large annealing intervals used or missing data. In this paper strong effort has been made to obtain a reliable RR spectrum, treating the whole uncertainties of a resistivity measurement in an explicit way because in literature this point is normally omitted.

3. BCA analysis of proton irradiation

As we mentioned in a previous section, resistivity measurements have been done in most investigations with electrons to understand the basic effects of radiation. In the case of fusion materials, it is necessary to model the effect of neutrons and therefore the damage and results obtained using electrons has to be extrapolated to the neutron case. As protons will produce a type of damage closer to the one generated by neutrons than electrons, it seemed to us that it would be interesting to extend RR results previously obtained by electron irradiation to the case of protons. This section presents a discussion concerning differences and similarities with neutron, proton and electron irradiations and the particular case here studied of 5 MeV protons on a Fe–5%Cr sample.

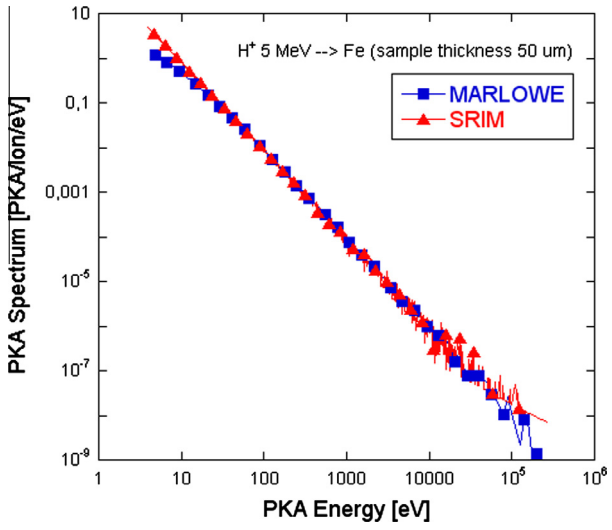

Fig. 4. PKA spectra of 5 MeV protons in 50 μm sample. Squares correspond to calculations made with MARLOWE code and triangles correspond to calculations made with SRIM code.

The 14 MeV fusion neutrons are expected to produce high energy recoils which will be responsible for the formation of a large amount of defects. High energy protons (10–18 MeV) would reproduce the high energy recoils but also would produce a higher number of low energy recoils which may end up in a larger proportion of FPs than in the case of neutron irradiation. Indeed, as it was shown by Omar et al. [36], the differential cross-sections and damage energy distributions of 10–16 MeV protons approximate to 14 MeV neutrons for energy recoils greater than few keV. However, protons deposit a larger fraction of their damage energy through collisions with energy transfers lower than 1 keV compared to neutrons. Thus, except in the low energy part, the PKA spectrum expected for high-energy protons is very similar to the one obtained with 14 MeV neutrons. The PKA spectrum of 5 MeV protons in a 50 μm Fe sample was calculated by using two independent BCA codes: SRIM and MARLOWE [37]. The results are plotted in Fig. 4 and good agreement between both calculations is observed. The obtained mean energy of PKA spectrum is about 0.35 keV. This value has to be compared for example to the case of 2.5 MeV electrons, which produce PKA's with a mean energy of only 0.06 keV [38]. Therefore, although it is expected that in both cases mainly FPs will form during irradiation, some differences could be expected. In particular, it seems reasonable to think that the created FPs will have a different spatial distribution, mainly a higher separation distance between the SIA and its vacancy than the one obtained with electron irradiation. Thus for 5 MeV protons, the I–V mean distance would be larger than the $4a_0$ calculated for 2.5 MeV electrons [39]. Following this reasoning, this larger separation would lead to a reduction of stage I amplitude for proton irradiated samples, as it is experimentally observed (see Section 5). The type of created damage and its spatial distribution is going to be of high importance for interpretation of the experimental results, in particular at low temperatures, where spatial correlations between defects play an important role, as demonstrated in [39].

As previous authors used SRIM to estimate the FP number, we also used this code for dose comparison purposes (it is well known that position of peaks can be dose dependent). For a proton irradiation in pure Fe, the obtained initial concentration of FPs was 100 appm for a fluence of 3.7×10^{15} cm^{-2}. Anyway total dose could also be compared by RIR values. We also assume that the concentration of FPs in Fe–Cr based alloys will be similar. Indeed, as it was shown by Terentyev et al. [4] using MD, the presence of Cr does not affect the ballistic phase of the cascades and eventually in terms of number of atomic displacements, volume and density and the final population of defects and clusters is only slightly altered. Models just predict a slight increase in the FP number and less defect clusters of $n > 5$. The main difference is that the concentration of the Cr dumbbells is higher than expected from sample

stoichiometry due to the recombination effects during the ballistic phase of the cascades. For more realistic calculations, including recombination, MARLOWE code was also used to estimate FP density, obtaining only 18 appm using the accepted capture radius of 3.3 a_o for *I*–*V* recombination [40].

4. Results

The experimental characteristics of the sample are given in Table 3, as well as the fluence and the RIR. The increase in resistivity as a function of proton fluence is plotted in Fig. 5 along with the resistivity change rate (RCR = $d\rho/d\phi$). As it has been observed in a previous work on Fe–Cr alloys [14], the rate of change of the resistivity decreases towards an asymptotic value, which is explained by the assumption that the defect specific resistivity is a decreasing function of defect concentration.

Table 3
Specimen experimental characteristics, residual resistivity ratio (RRR) and RIR measured at minimum temperature reached on the sample, 23 K.

Sample	Thickness (μm)	ρ_0 ($n\Omega$ cm)	RRR	Fluence (ion/cm^2)	$\Delta\rho$ ($n\Omega$ cm)
Fe–5%Cr	51.83 ± 1.17	9893.0 ± 0.6	3.3	3.7×10^{15}	431

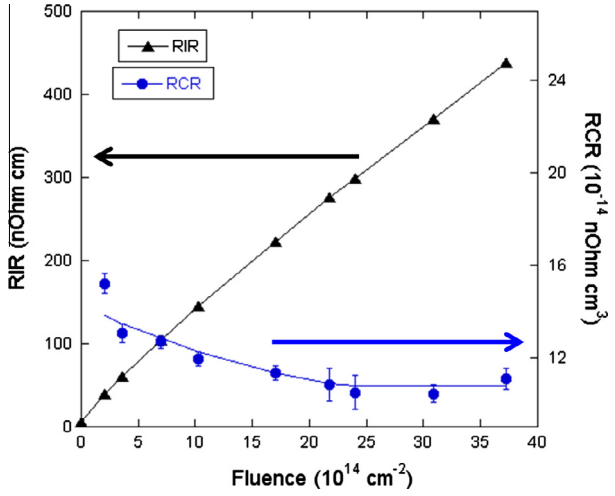

Fig. 5. Radiation induced resistivity of Fe–5%Cr measured at T_{min} = 23 K (triangles – left axis) and the corresponding resistivity change rate (dots – right axis).

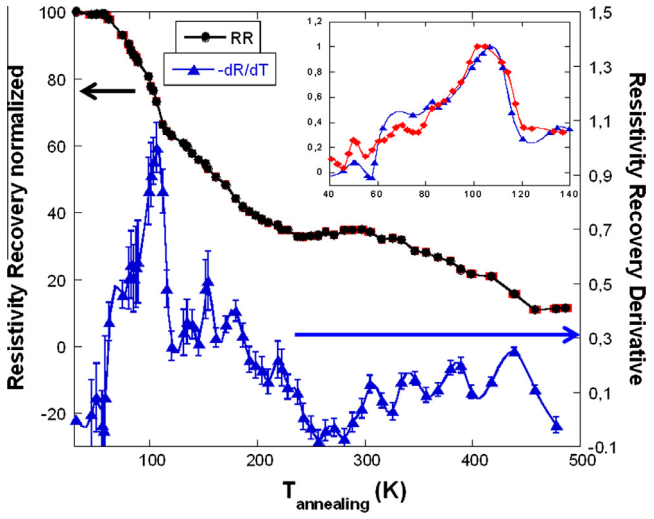

Fig. 6. Isochronal recovery $\Delta\rho(T)/\Delta\rho_0$ and its derivative, $-d(\Delta\rho(T)/\Delta\rho_0)/dT$ for Fe–5%Cr alloy.

In Fig. 6 we reported the variation of the normalized RR (RR = $\Delta\rho/\Delta\rho_0$) with annealing temperature for the Fe–5%Cr as explained in Section 2.3. The RR values shown in this figure are normalized at T_{base}. Details on the calculation of the errors were described is Section 2.3. For the sake of clarity the RR derivative has been also depicted in Fig. 6. It can feel striking to the reader that the uncertainties in RR derivative get reduced as the annealing rises temperatures, but this comes from the used error formula itself. As it is a derivative, it takes into account the temperatures difference between each pair of points. At very low temperature, the points are very close, so dividing by this difference gives higher numerical errors, different from purely experimental errors. Paradoxically, the more spaced are the points in the annealing, the lower error in derivative is provided, although some information is lost in between. Despite of this, it has been considered that high resolution in temperature is better to reveal the fine structure of the RR peaks.

5. Discussion

For the analysis of the experimental RR spectrum the determination of the temperature range of each stage was made following previous works carried out on Fe and $FeCr_x$ alloys [5,11,20] but adapted to the current measurement. The definition of the intervals and % of recovery for every stage is detailed in Table 4, and compared to the works of Nikolaev [17] and Benkaddour et al. [20] (both electron irradiation) obtained after digitalization of their results. To compare with previous results, a convention has been followed regarding stage notation; stage III_A corresponds to the generally accepted stage III, the notation III_B corresponds to the temperature interval up to what we can compare with Nikolaev's data and stage III_C corresponds to the rest of the temperature range beyond stage III and before stage IV (520–550 K) [10]. As it can be seen in Fig. 6, the RR spectrum obtained with the Fe–5%Cr sample exhibits stages I, II and III in the temperature intervals at which they have been already observed in the literature [17,20] on samples irradiated with 5 and 2.5 MeV electrons (reaching values of RIR of 380 and 3333 $n\Omega$ cm, respectively). A graphical comparison of such measurements can be found in Figs. 7 and 8.

As it is evidenced in Fig. 6, stage I is in fact a result of several sub-stages. Our results are in agreement with the accepted view that stage I in Fe–Cr alloys corresponds in fact to correlated recombination of SIAs and mixed dumbbells with vacancies. The main recovery is found at 108 K and corresponds to the I_D substage process that is usually observed in pure Fe. Peaks or shoulders below 108 K have been related to close pair recombination of non-trapped mixed dumbbells which have a lower migration energy (E_m = 0.23 eV [41]) than SIA (E_m = 0.34 eV [41,42]) and even mixed DI-SIA (Fe–Fe and Cr–Cr dumbbell) with an estimated activation energy of 0.30 eV [41] for a dilute FeCr system. Using sufficiently small annealing steps we were able in this work to reveal a substructure of stage I around, 50, 70 and 80 K. Concerning the relative amplitude of stage I, as the mean distance between the FPs is expected to be larger than in electron irradiation experiments, as already discussed in Section 3, configurational trapping [16,39] has higher influence, Thus less recovery due to correlated recombination is expected in proton irradiated alloys. Indeed this is confirmed by the partial recovery in stage I indicated in Table 4.

In Fe–Cr systems the long-range migration of SIAs and mixed dumbbells is suppressed in stage I by the trapping effect of other neighbouring Cr_s atoms (substitutional Cr). Thus formation of clusters of 2 or 3 SIAs (E_m = 0.43 eV [41]) is also suppressed and the

Table 4
Percent recovery of resistivity in every stage along thermal annealing.

Stage I (30–120)	Stage II (120–200)	Stage III_A (200–285)	Stage III_B (285–400)	Stage III_C (400–485)	Incident particle and energy	Source
37.0	24.2	4.1	13.1	10.2	H^+ 5 MeV	Present work
58.6	18.6	16.6	2.1	–	e^- 5 MeV	Nikolaev [17]
53.7	27.6	11.4	3.2	2.1	e^- 2.5 MeV	Benkaddour et al. [20]

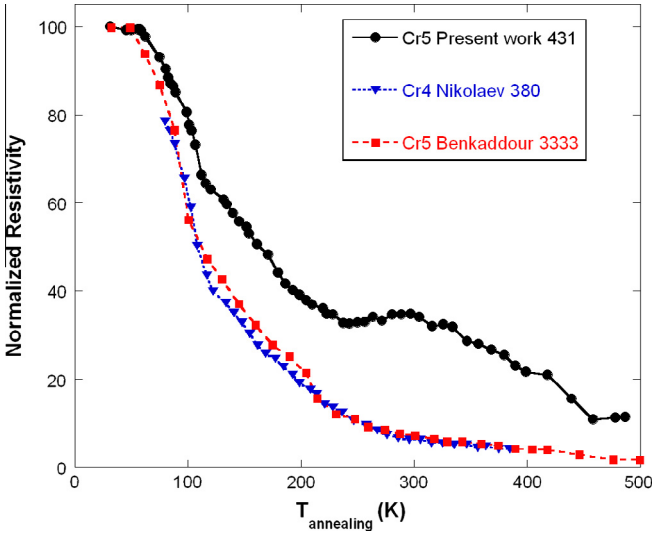

Fig. 7. Representation of the defect recovery curve in Fe–5%Cr irradiated with 5 MeV protons (this work), together with digitalized data from experiments made with 5 and 2.5 MeV electrons in samples with 4% and 5% of Cr respectively [17,20].

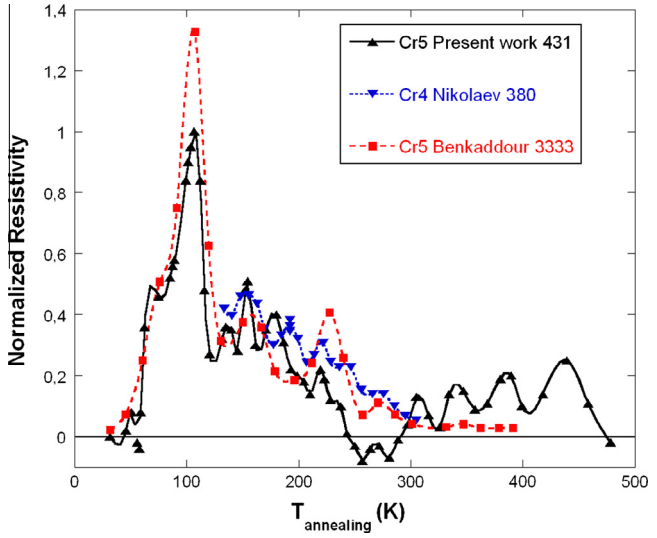

Fig. 8. Comparison of the RR spectra curves of Fe–5%Cr irradiated with 5 MeV protons (this work), with digitalized data from experiments made with 5 and 2.5 MeV electrons in samples with 4% and 5% of Cr respectively [17,20].

presence of stage II cannot be attributed anymore to migration of such clusters, as it is in pure Fe [10] except to those created during irradiation if it is the case. The existing literature presents controversies in the interpretation of stage II. Some authors attribute it to long range migration of SIAs which dissociate from configurational trapping at effective energies of 0.40–0.45 eV in concentrated alloys [39]. This result is based on experimental results from Benkaddour and Dimitrov [11,20] who observed a single well defined peak. According to Figs. 6 and 8, in our case stage II appears to be composed of a set of three small peaks or sub-stages. In the case of Benkaddour's curve, it could be attributed to a too high smoothing of experimental data or low resolution, which would wipe out variations in RR. On the other hand, Nikolaev's curve also shows two peaks in this temperature interval. One at 155 K and the other at 195 K which he associates to correlated migration of vacancies. Thus, present result strongly supports the existence of such substructure, i.e. that it will be showing differentiated migration mechanisms all associated to the stage II. Future measurements and simulations will confirm or refute the appearance of these sub-stages and their underlying processes.

Nikolaev has also claimed that the onset of free vacancy migration, which is the characteristic of stage III, occurs in Fe–Cr alloys at 195 K [19]. In the case of binary alloys, the long range migration of defects enhances rearrangement of solutes, i.e. produces SRO effects which change the residual resistivity. In particular, it has been argued that free vacancy migration is very effective at altering SRO [43]. It is worth noting that in the case of electron irradiation, no effect of SRO contributions was observed in conventional RR curves in Fe–4%Cr and Fe–5%Cr [17]. A specific approach is required to observe the SRO contributions in such samples [19]. In the present work, at this temperature, the proton irradiated RR curve starts to deviate from the electron irradiated ones (see Fig. 7). This temperature coincides with the end of stage II at the present RR derivative curve (Figs. 6 and 8). It is also observed that the characteristic peaks previously found in the RR derivative by other authors [17,20] after the onset of long range vacancy migration almost disappear in the present RR spectrum. It seems that the recombination stages are hidden. In our case it is measured that in this temperature interval only a 4% RR occurs in our sample while the partial recovery on electron irradiated samples is 16–11%. Moreover, the RR rate becomes negative at the end of III_A. This is very likely due to an increase in the SRO effects in the proton irradiated sample, which in the case of Fe–5%Cr, contribute to increase the residual resistivity of the sample [12]. This inversion of the RR is in fact attributed to an increase in resistivity by the Cr ordering in the alloy [12]. A mechanism that might promote the short-range rearrangement of Cr atoms in the vicinity of trapped defects has been recently described and depicted by Nikolaev (Figs. 6 and 7 of [18]) for vacancy–carbon defects. The present results suggest that a similar mechanism with trapped dumbbells and Vs should operate in the case of non C-doped Fe–4Cr samples. The proposed model assumes that during its migration, the vacancy can exchange its position with a neighbouring Fe or Cr atom, depending on which one is more energetically favourable. The probable path is determined by the specific number and spatial distribution of nearest-neighbours (nn) and next-nn Cr atoms. Thus, a local arrangement of atoms can be reordered as the vacancy migrates in the vicinity, favouring the system to go to equilibrium value in terms of SRO (at this temperature).

Such significant SRO effect is possible given that, as it has been observed by Mössbauer Spectroscopy measurements, the distribution of Cr atoms in $Fe_{100-x}Cr_x$ alloys with $x \leqslant 25$ is not random but instead has a particular atomic configuration [44]. In addition, beyond stage III, at 220 K the long range migration of de-trapped SIAs also starts [18] and this migration could also contribute to the SRO

(although vacancies are more effective). At the highest annealing temperatures (485 K) there is still a 10% of recovery remaining, indicating that the Cr configuration is not the same as before irradiation and that there is still some SRO contribution to the resistivity induced by irradiation. Recovery peaks observed beyond 250 K are still of unknown nature, but their differences with respect to smooth derivative of Benkaddour could be explained by a difference in radiation damage.

Therefore it seems that proton irradiation, besides producing a different damage distribution and type than electrons, also favours the appearance of SRO effects in RR curves. Damage distribution and type, i.e. small cascades or presence of small clusters, might also play a role in the number of peaks and their position. Other aspects related to the sample microstructure such as its impurity content, dislocation density or initial Cr distribution could also be the responsible for some of the observed differences (as indicated, our sample is of higher purity).

6. Conclusions

In this contribution, the recently developed set-up for low temperature resistivity measurements of ion-irradiated samples has been detailed in order to apply it to nuclear reactor materials study. Experimental errors and measurement procedure to obtain reliable RR data were presented and discussed.

The presentation and analysis of the data relative to RR of an Fe–5%Cr alloy has not only confirmed the good performance of the presented set-up, but also have raised intriguing questions about the behaviour of Fe–Cr systems under irradiation. For example, SRO effects seem to be much stronger in proton-irradiated samples than under electron irradiation, leading mainly to an important reduction of stage III (200–285 K), then followed by an increase of RR rate at higher temperatures (up to 450 K). The role of the different PKA mean energy obtained in the present work compared to previous works on electron irradiations has been discussed, which could explain some differences on peak positions/heights. Further work on higher Cr content alloys and a different approach to suppress SRO from RR measurement is in progress, which will allow us to obtain a better understanding of basic mechanisms of FeCr evolution under irradiation.

Acknowledgements

This work has been co-supported by the European Commission (EFDA – MATREMEV workprogram) and Euratom/CIEMAT Association, JCI-2009-05681, and by Madrid Community through the Project TECHNOFUSION (S2009/ENE-1679).

The authors are grateful to Dr. M.A. Ramos (UAM, Spain), Dr. G. Apostolopoulos (NCSR DEMOKRITOS, Greece), Dr. K. Murakami (University of Tokyo, Japan) and Dr. P. Fernández (CIEMAT, Spain) for helpful discussions about the experimental work and to Dr. K. McCarthy and Dr. I. García-Cortés (CIEMAT, Spain) for helpful corrections on the manuscript.

References

[1] Y.V. Konobeev, A.M. Dvoriashin, S.I. Porollo, F.A. Garner, J. Nucl. Mater. 355 (2006) 124.
[2] H. Kayano, A. Kimura, M. Narui, Y. Sasaki, Y. Suzuki, S. Ohta, J. Nucl. Mater. 155–157 (1988) 978.
[3] M. Dusek, C. Hunt, Test Methods for Evaluating the Reliability of PCB Finishes Using Lead-Free Alloys – a Guide, NPL Report MATC(A)90, 2002.
[4] D.A. Terentyev, L. Malerba, R. Chakarova, K. Nordlund, P. Olsson, M. Rieth, J. Wallenius, J. Nucl. Mater. 349 (2006) 119.
[5] S. Takaki, J. Fuss, H. Kuglers, U. Dedek, H. Schultz, Radiat. Eff. 79 (1983) 87.
[6] F. Maury, A. Lucasson, P. Lucasson, Y. Loreaux, P. Moser, J. Phys. F: Metal Phys. 16 (1986) 523.
[7] H. Matsui, S. Takehana, M.W. Guinan, J. Nucl. Mater. 155–157 (1988) 1284.
[8] A.L. Nikolaev, V.L. Arbuzov, A.E. Davletshin, J. Phys.: Condens. Matter 9 (1997) 4385.
[9] A. Vehanen, P. Hautojärvi, J. Johansson, J. Yli-Kauppila, P. Moser, Phys. Rev. B 25 (1982) 762.
[10] C.-C. Fu, J. Dalla, Nat. Mater. 4 (2005) 68.
[11] C. Dimitrov, A. Benkaddour, C. Corbel, P. Moser, Ann. Chim.-Sci. Mat. 16 (1991) 319.
[12] I. Mirebeau, M. Hennion, G. Parette, Phys. Rev. Lett. 53 (1984) 687.
[13] I. Mirebeau, G. Parette, Phys. Rev. B 82 (2010).
[14] F. Maury, P. Lucasson, A. Lucasson, F. Faudot, J. Bigot, J. Phys. F: Metal Phys. 17 (1987) 1143.
[15] H. Abe, E. Kuramoto, J. Nucl. Mater. 271–272 (1999) 209.
[16] A.L. Nikolaev, J. Phys.: Condens. Matter 11 (1999) 8633.
[17] A.L. Nikolaev, Philos. Mag. 87 (2007) 4847.
[18] A.L. Nikolaev, Philos. Mag. 91 (2011) 879.
[19] A.L. Nikolaev, Philos. Mag. 89 (2009) 1017.
[20] A. Benkaddour, O. Dimitrov, C. Dimitrov, Mater. Sci. Forum 15–18 (1987) 1263.
[21] V. Arbuzov, B. Goshchitskii, V. Sagaradze, S. Danilov, A. Kar'kin, Phys. Metals Metallogr. 110 (2010) 366.
[22] A. Climent-Font, F. Pászti, Nucl. Instrum. Methods Phys. Res. Sect. B 219–220 (2004) 400.
[23] ASTM F76-86, Test Methods for Measuring Resistivity and Hall Coefficient and Determining Hall Mobility in Single-Crystal Semiconductors, ASTM International, 1996.
[24] D.A. Thompson, A.M. Omar, J.E. Robinson, J. Nucl. Mater. Part 1 85–86 (1979) 509.
[25] O. Dimitrov, C. Dimitrov, J. Nucl. Mater. 105 (1982) 39.
[26] <http://www.efda.org/>, n.d.
[27] J. Le Coze, Procurement of Pure Fe Metal and Fe-Based Alloys with Controlled Chemical Alloying Element Contents and Microstructure, ARMINES Ecole Nationale Superieure des Mines, 2007.
[28] L.J. van der Pauw, Philips Res. Rep. 13 (1958) 1.
[29] X. Huang, C. Gao, Y. Han, M. Li, C. He, A. Hao, D. Zhang, C. Yu, G. Zou, Y. Ma, Appl. Phys. Lett. 90 (2007) 242102.
[30] X. Huang, C. Gao, D. Zhang, M. Li, C. He, A. Hao, C. Yu, C. Sang, C. Liu, Y. Wang, R. Guan, D. Li, G. Zou, Y. Ma, Appl. Phys. Lett. 90 (2007) 204102.
[31] Y. Sun, J. Shi, Q. Meng, Semicond. Sci. Technol. 11 (1996) 805.
[32] J.F. Ziegler, Nucl. Instrum. Methods Phys. Res. Sect. B 219–220 (2004) 1027.
[33] L.E. Samuels, Metallographic Polishing by Mechanical Methods, fourth ed., ASM International, Materials Park, OH, 2003.
[34] G.F. Vander Voort, ASM Handbook, Metallography and Microstructures, vol. 09, ASM International, Materials Park, OH, 2004.
[35] A. Daire, Low-Voltage Measurement techniques, Keithley Report, 2005.
[36] A.M. Omar, J.E. Robinson, D.A. Thompson, J. Nucl. Mater. 64 (1977) 121.
[37] M. Robinson, I. Torrens, Phys. Rev. B 9 (1974) 5008.
[38] A. Iwase, T. Hasegawa, Y. Chimi, T. Tobita, N. Ishikawa, M. Suzuki, T. Kambara, S. Ishino, Nucl. Instrum. Methods Phys. Res. Sect. B 195 (2002) 309.
[39] D. Terentyev, N. Castin, C.J. Ortiz, J. Phys.: Condens. Matter 24 (2012) 475404.
[40] A. Souidi, M. Hou, C.S. Becquart, C. Domain, J. Nucl. Mater. 295 (2001) 179.
[41] C.J. Ortiz, D. Terentyev, P. Olsson, R. Vila, L. Malerba, J. Nucl. Mater. 417 (2011) 1078.
[42] C.-C. Fu, F. Willaime, P. Ordejón, Phys. Rev. Lett. 92 (2004).
[43] K. Kohl, W. Scheffel, R. Heidsiek, H. Lücke, Acta Metall. 31 (1983) 1895.
[44] S.M. Dubiel, J. Cieslak, Phys. Rev. B 83 (2011) 180202.